

# What if the Doyle-Fuller-Newman model fails? A new macroscale modeling framework

Harikesh Arunachalam, *Member, IEEE* and Simona Onori\*, *Senior Member, IEEE*

**Abstract**—The Doyle-Fuller-Newman (DFN) model is generally considered the modeling standard to assess the worthiness of reduced-order electrochemical models. An aspect of such a macroscale model which has often been overlooked is that they are approximate representations of pore-scale transport dynamics and their predictive ability is hence susceptible to certain operating conditions. In this paper, we identify battery operating conditions that lead to loss of accuracy and root mean square error as high as 83.9 mV in the voltage prediction of the DFN model, and interpret our observations using a phase diagram analysis. Under the same scenarios, we simulate the performance of a full-homogenized macroscale (FHM) model developed by applying multiple-scale expansions to the Poisson-Nernst-Planck (PNP) transport equations. The performance of both models is assessed against experiments conducted on 18650 cylindrical lithium-ion cells. Results infer that the DFN model fails to predict battery voltage accurately towards the end of discharge at temperatures higher than 40°C. The FHM model accurately predicts measured battery terminal voltage with less than 22 mV RMS error for the evaluated conditions.

## NOMENCLATURE

$\eta_e$	Electrolyte volume fraction [–]
$\eta_s$	Active material volume fraction [–]
$\bar{\phi}_s$	Averaged electrode phase potential [V]
$\bar{\phi}_e$	Averaged electrolyte phase potential [V]
$a$	Electrode specific surface area [ $m^{-1}$ ]
$A_{cell}$	Electrode cross-sectional area [ $m^2$ ]
$c_s$	DFN model electrode concentration [ $molm^{-3}$ ]
$c_{s,max}$	Electrode saturation concentration [ $molm^{-3}$ ]
$c_{s,surf}$	Electrode surface concentration in the DFN model [ $molm^{-3}$ ]
$\bar{c}_e$	Electrolyte average concentration [ $molm^{-3}$ ]
$\bar{c}_s$	Electrode average concentration in the FHM model [ $molm^{-3}$ ]
$D_e$	Pore-scale electrolyte diffusion coefficient [ $m^2s^{-1}$ ]
$D_{e,j}^{eff}$	Effective electrolyte diffusion coefficient [ $m^2s^{-1}$ ]
$D_s$	DFN model active material diffusion [ $m^2s^{-1}$ ]
$D_s^{eff}$	Effective electrode diffusion coefficient in the FHM model [ $m^2s^{-1}$ ]
$F$	Faraday constant [ $Vs\Omega^{-1}mol^{-1}$ ]
$I_{app}$	Applied current [A]
$J_{Li}$	Intercalation current density [ $A/m^3$ ]
$k$	Reaction rate in the DFN model [ $Am^{2.5}mol^{-1.5}$ ]
$k^*$	Reaction rate in the FHM model [ $A/mol$ ]
$K_e$	Pore-scale electrolyte conductivity [ $S^{-1}m^{-1}$ ]
$K_e^{eff}$	Effective electrolyte conductivity [ $S^{-1}m^{-1}$ ]

$K_s^{eff}$	Effective electrode conductivity [ $S^{-1}m^{-1}$ ]
$L_n$	Thickness of the anode [ $m$ ]
$L_p$	Thickness of the cathode [ $m$ ]
$L_s$	Thickness of the separator [ $m$ ]
$r$	Radial coordinate direction [ $m$ ]
$R$	Universal gas constant [ $Jmol^{-1}K^{-1}$ ]
$R_c$	Contact resistance at the current collectors [ $\Omega$ ]
$t_+$	Transference number [–]
$T$	Cell temperature [K]
$x$	Cartesian coordinate direction [ $m$ ]
$x_{n,init}$	Initial anode stoichiometric coefficient [–]
$x_{p,init}$	Initial cathode stoichiometric coefficient [–]

## I. INTRODUCTION

The transportation sector has witnessed many technological advancements in recent years to enhance fuel efficiency and reduce vehicular emissions [1]. Among these technologies, electrification of the vehicle powertrain has been widely implemented in the automotive industry. Lithium-ion batteries, electrochemical energy storage devices, are the most preferred technology today for electric and hybrid propulsion systems. Despite the decreasing cost of lithium ion battery packs over the years [2], growth of the global electric vehicle market has been slower than initially predicted [3].

Lithium-ion battery packs used in automotive applications today are oversized and underutilized to meet vehicle life expectancy. This conservative strategy has resulted in heavier and expensive battery systems. The transition to large scale applications has been hampered by the relative lack of understanding of scaling effects, which impact battery performance and electrochemical and mechanical responses [4].

Safe, efficient battery utilization for large-scale applications is possible using a sophisticated battery management system (BMS). To optimize performance and prolong battery useful life, accurate estimation of battery state-of-charge (SoC) and prediction of the battery state-of-health (SoH) is required [5]. This depends on the mathematical models describing lithium transport and the precision with which their parameters are measured, estimated, or identified [6]. Advanced electrochemical modeling and estimation of battery internal states are vital to push batteries to operate at their physically permissible limits [7].

Lithium-ion batteries involve highly non-linear transport processes at multiple length scales [8]. As such, ion transport can also be modeled on a multiplicity of length scales. Models characterizing battery behavior at the smaller length scales capture battery behavior better because they rely on fundamental first principles to describe the transport

H. Arunachalam and S. Onori are with the Department of Energy Resources Engineering, Stanford University, Stanford, CA, 94305, USA. harunac@stanford.edu, sonori@stanford.edu

\* corresponding author

DFN Model	FHM Model
Electrode Mass Transport Equation	
$\frac{\partial c_{s,j}(x,r,t)}{\partial t} = \frac{D_{s,j}}{r^2} \left( r^2 \frac{\partial c_{s,j}(x,r,t)}{\partial r} \right), \quad j = (n, p)$	$\frac{\partial \bar{c}_{s,j}}{\partial t} = D_{s,j}^{eff} \frac{\partial^2 \bar{c}_{s,j}}{\partial x^2} - \frac{1}{F} J_{Li,j}(x, t), \quad j = (n, p)$
Electrolyte Mass Transport Equation	
$\eta_{e,j} \frac{\partial \bar{c}_{e,j}(x,t)}{\partial t} = \frac{\partial}{\partial x} \left( D_{e,j}^{eff} \frac{\partial \bar{c}_{e,j}(x,t)}{\partial x} \right) + \frac{(1-t_+)}{F} J_{Li,j}(x, t), \quad j = (n, s, p)$	$\eta_{e,j} \frac{\partial \bar{c}_{e,j}}{\partial t} = D_{e,j}^{eff} \frac{\partial^2 \bar{c}_{e,j}}{\partial x^2} + \frac{RTt_+^2}{F^2} K_{e,j}^{eff} \frac{\partial^2 \ln \bar{c}_{e,j}}{\partial x^2} + \frac{t_+}{F} K_{e,j}^{eff} \frac{\partial^2 \bar{\phi}_{e,j}}{\partial x^2} + \frac{1}{F} J_{Li,j}(x, t), \quad j = (n, s, p)$
Electrode Charge Transport Equation	
$K_{s,j}^{eff} \frac{\partial^2 \bar{\phi}_{s,j}(x,t)}{\partial x^2} = J_{Li,j}(x, t), \quad j = (n, p)$	$K_{s,j}^{eff} \frac{\partial^2 \bar{\phi}_{s,j}}{\partial x^2} = J_{Li,j}(x, t), \quad j = (n, p)$
Electrolyte Charge Transport Equation	
$-K_{e,j}^{eff} \frac{\partial^2 \bar{\phi}_{e,j}(x,t)}{\partial x^2} - \frac{2K_{e,j}^{eff} (x,t) RT(1-t_+)}{F} \frac{\partial^2 \ln \bar{c}_{e,j}}{\partial x^2} = J_{Li,j}(x, t), \quad j = (n, s, p)$	$\frac{RTt_+}{F} K_{e,j}^{eff} \frac{\partial^2 \ln \bar{c}_{e,j}}{\partial x^2} + K_{e,j}^{eff} \frac{\partial^2 \bar{\phi}_{e,j}}{\partial x^2} = -J_{Li,j}(x, t), \quad j = (n, s, p)$
Intercalation Current Density	
$J_{Li,j}(x, t) = a_j k_j \sqrt{c_{s,surf,j} \cdot (c_{s,max,j} - c_{s,surf,j})} \cdot \sqrt{\bar{c}_{e,j}(x, t)} \cdot 2 \sinh \left[ \frac{0.5F}{RT} (\bar{\phi}_{s,j} - \bar{\phi}_{e,j} - U_{0,j}) \right], \quad j = (n, p)$ $J_{Li,s}(x, t) = 0$	$J_{Li,j}(x, t) = k_j^* \cdot \sqrt{\bar{c}_{e,j} \cdot \bar{c}_{s,j} \cdot \left( 1 - \frac{\bar{c}_{s,j}}{c_{s,max,j}} \right)} \cdot 2 \sinh \left( \frac{F}{2RT} [\bar{\phi}_{s,j} - \bar{\phi}_{e,j} - U_{0,j}] \right), \quad j = (n, p)$ $J_{Li,s}(x, t) = 0, \quad \text{because the separator does not contain any active particles}$

TABLE I: Transport equations of the DFN and FHM models to describe lithium-ion transport dynamics.

processes. Lithium-ion transport can be captured at the microscopic length scales using robust pore-scale models. However, their computational intensity renders them impractical as a predictive tool at the system level. Macroscopic models, which are approximate representations of the pore-scale physics, are particularly appealing for control and estimation strategies.

The electrochemical models used today have been derived from the work of Doyle *et. al.* [9]. Since its development, the DFN model has been accepted with limited criticism and debate as the most reliable physics-based modeling tool lithium-ion batteries. Its limitations in predicting battery dynamics at operating conditions characterized by high discharge rates and operating temperatures, and most importantly, aging, has not been adequately addressed. This is attributed to the fact that the battery operating regimes that lead to violation of the approximations and constraints that facilitated the development of the DFN model have not been well documented in published literature.

Some of the underlying assumptions of the DFN model are summarized in [10], [11]. The most critical among them concerns the particle geometry. Experimental investigations [12] have proven that practical battery electrodes have non-spherical particle shapes which exhibit polydispersity. Moreover, the effective transport properties are obtained using an empirical relation that depends only on the electrolyte volume fraction. However, electrode topology and morphology play a significant role in influencing these ef-

fective properties [13]. Such limitations may be significantly amplified in the single particle models [14], [15].

As a result, the performance of such control-oriented models may not accurately reflect real-world battery response even though their performance is accurate with respect to the DFN model. Thus far, research efforts have not completely tackled the problem of identifying the right conditions of operation of the models that are being utilized. Unless this is addressed, lack of awareness of model utilization may lead to its implementation for the wrong applications.

This discussion in no manner intends to undermine previous modeling contributions. The DFN model has been invaluable in the development of model-based strategies for estimation, control, and diagnostics. Rather, in the quest of understanding how to design and utilize batteries effectively, this section serves to highlight specific attributes that are missing in macroscale transport models, and motivates the work presented in this paper.

This paper is structured as follows: Section II summarizes the numerical implementation of the DFN and the FHM models. Section III describes the parameter identification approach for the DFN and FHM models. The particle swarm optimization (PSO) algorithm is used for the identification studies conducted in this work. Section IV discusses the outcome of the identification studies. Section V summarizes the conclusions of this work.

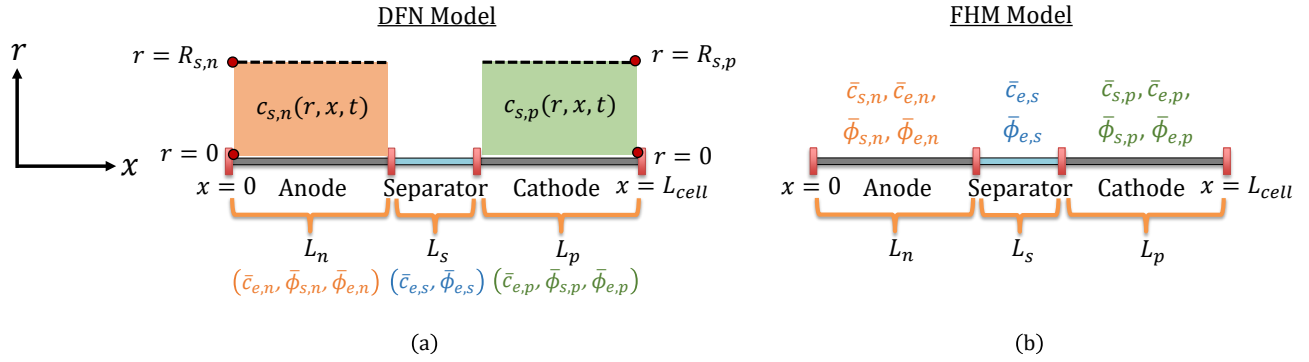


Fig. 1: DFN and FHM model variables. As shown in (a),  $c_s$  is resolved in a pseudo radial direction in the electrodes, and the other variables are resolved in the  $x$  direction. The variables of the FHM model, shown in (b), are resolved along  $x$ .

## II. FINITE ELEMENT IMPLEMENTATION

### A. DFN Model

The transport equations of the DFN and FHM models are summarized in Table I.  $n$ ,  $s$ , and  $p$  represent the anode, separator, and cathode, respectively. A detailed comparison analysis of the mass and charge transport equations of the DFN and the FHM models is presented in [16]. The finite element implementation of the DFN model was conducted by Plett *et. al* [17].

As illustrated in Fig. 1, this is a *pseudo two-dimensional* battery model since the electrode mass conservation equation for  $c_s$  is resolved in a *pseudo* radial direction,  $r$ , while the remaining variables  $\bar{\phi}_s$ ,  $\bar{\phi}_e$ , and  $\bar{c}_e$  are resolved along the direction perpendicular to the current collectors,  $x$ . The non-linear partial differential equations (PDEs) of the DFN model are coupled through the intercalation current density. In addition to this coupling, the electrolyte charge conservation equation consists of both the electrolyte concentration and potential variables.

### B. FHM Model

The finite element implementation of the FHM model [18] using COMSOL Multiphysics<sup>®</sup> facilitates the comparison studies on the two macroscale models using the same computational platform. Taking into consideration that an unbiased comparison must be made, the FHM model is developed in a one-dimensional setting. The equations of the FHM model are summarized in Table I.

Electrolyte diffusion and conductivity are represented by concentration-dependent entities  $D_e^{eff}$  and  $K_e^{eff}$ , respectively. It must be noted in the FHM model that both the electrolyte mass and charge conservation equations consist of the electrolyte concentration and potential variables.

### C. General Remarks

The terminal voltage of the cell in the DFN and the FHM models is evaluated using the expression:

$$V(t) = \bar{\phi}_{s,p}(L_{cell}, t) - \bar{\phi}_{s,n}(0, t) - R_c \cdot I_{app}(t), \quad (1)$$

where  $R_c$  is the contact resistance at the current collectors. This is the model-predicted voltage output that is compared

with the experimentally measured cell terminal voltage response.

The open circuit potential curve for the graphite anode and nickel manganese cobalt oxide (NMC) cathode were obtained from [15]. Pore-scale electrolyte diffusion and conductivity coefficients as a function of concentration and temperature were obtained from [19]. Effective diffusion and conductivity for the DFN model were obtained using the Bruggeman approach [20], and by resolving the closure problem for the FHM model [16].

## III. MODEL PARAMETER IDENTIFICATION

This section elaborates upon the identification studies conducted to determine the parameters of the DFN and the FHM models using an integrated Matlab<sup>®</sup> and COMSOL Multiphysics<sup>®</sup> co-simulation framework. For an elaborate description of the development of the FHM model and the parameter identification studies, the reader is referred to [21].

The parameters of both models were identified by selecting a specific experimental data set and minimizing the error between the measured voltage response and the model-predicted voltage for the given current input. A total of 18 parameters of the DFN and FHM models were identified using experimental data, with the vector of parameters being:

$$\theta_{DFN} = [L_n \ L_s \ L_p \ A_{cell} \ D_{s,n} \ D_{s,p} \ k_n \ k_p \ R_c \ x_{n,init} \ x_{p,init} \ c_{s,max,n} \ c_{s,max,p} \ \eta_n \ \eta_p \ \eta_{e,n} \ \eta_{e,s} \ \eta_{e,p}]^T \quad (2)$$

for the DFN model and

$$\theta_{FHM} = [L_n \ L_s \ L_p \ A_{cell} \ D_{s,n}^{eff} \ D_{s,p}^{eff} \ k_n^* \ k_p^* \ R_c \ x_{n,init} \ x_{p,init} \ c_{s,max,n} \ c_{s,max,p} \ \eta_n \ \eta_p \ \eta_{e,n} \ \eta_{e,s} \ \eta_{e,p}]^T \quad (3)$$

for the FHM model. The vector of parameters for both the models are identified using the PSO algorithm [22]. The objective of the parameter identification study is to determine the values of the 18 parameters by minimizing the cost

Parameter	DFN Model Identified Value	FHM Model Identified Value	Average
$L_n$ [m]	$50.60e - 6$	$51.60e - 6$	$51.1e - 6$
$L_s$ [m]	$31.0e - 6$	$24.9e - 6$	$28e - 6$
$L_p$ [m]	$40.8e - 6$	$39.4e - 6$	$40.1e - 6$
$A_{cell}$ [m <sup>2</sup> ]	0.1058	0.1026	0.1042
$x_{n,init}$ [-]	0.7878	0.7748	0.7813
$x_{p,init}$ [-]	0.3507	0.3402	0.3455
$c_{s,max,n}$ [mol/m <sup>3</sup> ]	29970	27611	28791
$c_{s,max,p}$ [mol/m <sup>3</sup> ]	46264	47852	47058
$\eta_{s,n}$ [-]	0.5813	0.6599	0.6206
$\eta_{s,p}$ [-]	0.5729	0.5724	0.5727
$\eta_{e,n}$ [-]	0.3037	0.2939	0.2988
$\eta_{e,s}$ [-]	0.4320	0.3888	0.4104
$\eta_{e,p}$ [-]	0.2841	0.3035	0.2938

TABLE II: The individually identified geometric and stoichiometric parameters of the DFN and FHM models, and their average values.

function; representing the root mean square errors:

$$J(\theta_k) = \sqrt{\left\{ \frac{1}{N} \sum_{i=1}^N \left( V_{exp}(i) - V_{mod}(\theta_k; i) \right)^2 \right\}}, \quad (4)$$

$k = \{DFN, FHM\}$ , where  $V_{exp}$  is the experimentally measured voltage response of the lithium-ion cell,  $V_{mod}$  is the model-predicted voltage that is a function of  $\theta_k$ ,  $N$  is the total number of data samples, and  $i$  is the time index.

The PSO-based identification is initiated by providing an initial guess for the elements of the vector  $\theta_k$ . A suitable initial guess and identification range for these elements is determined based on values reported in literature [15] and refined for each parameter. The radius of the active particles in the anode and cathode were kept constant at a value of 5  $\mu\text{m}$  for both the models. The model parameter identification approach is implemented as follows:

- 1) Step 1: The parameter identification study is initiated with a swarm population size of 200 and 10 generations. The termination criteria is 2200 iterations.
- 2) Step 2:  $\theta_k$  is identified for both models using 2A constant current capacity test in discharge experimental data conducted at 23°C. The anode and cathode conductivity coefficients, obtained from [23], were kept constant since prior studies [24] observed that they had no impact on the model-predicted response. Their values were unchanged in the identification studies.
- 3) Step 3: The geometric and stoichiometric parameters identified for the DFN and FHM models were averaged to enable unbiased simulations and identification studies. The averaged values of these 13 parameters are used in both the models, and are summarized in Table II.
- 4) Step 4: The 13 averaged parameters are invariant to

temperature, and are kept fixed for the subsequent identification studies. Since the averaging of parameters compromises the predictability of both the models, the identification study in Step 1 is repeated to optimize the remaining 5 parameters: the two electrode diffusion coefficients, the two reaction rate constants, and the contact resistance.

- 5) Step 5: In subsequent studies, only the aforementioned 5 parameters are identified as a function of temperature using 2A constant current discharge experimental data sets. The data sets for the identification studies reported in this paper were obtained from experiments at cell temperatures of 23°C, 40°C, and 45°C. The same cost function is utilized in all the identification studies.

The parameter identification studies were conducted on a Dell Precision T5810 desktop computer with 32.0 GB random access memory and Intel(R) Xeon(R) CPU E5-1650 v3 3.50 GHz processor. The parameter identification study using the FHM model and 23°C data took 65,048 s to complete, while the DFN model identification study using the 23°C data took 86,709 s to complete. The longer simulation time per iteration of the DFN model is attributed to the resolution of the model variables in two computational domains (radial and linear).

#### IV. RESULTS AND DISCUSSION

The performance of the DFN and FHM models for the identification studies conducted using 23°C, 40°C, and 45°C data sets is presented in Fig. 2. It must be noted that the five temperature-dependent parameters, which were individually identified for both the models, were kept separate and no further averaging of these parameters was performed while assessing model performance. Both the models predict battery behavior within an RMS error of 22 mV at 23°C. At

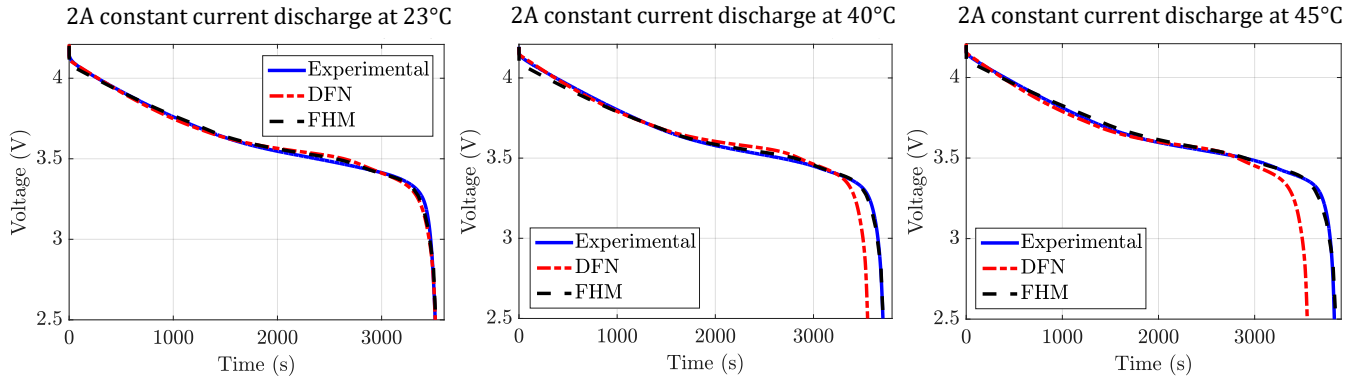


Fig. 2: Performance of the two models. The FHM model RMS error at 23°C, 40°C, and 45°C is respectively 21.6 mV, 21 mV, and 19 mV. The DFN model RMS error at these temperatures is respectively 22 mV, 75.8 mV, and 83.9 mV.

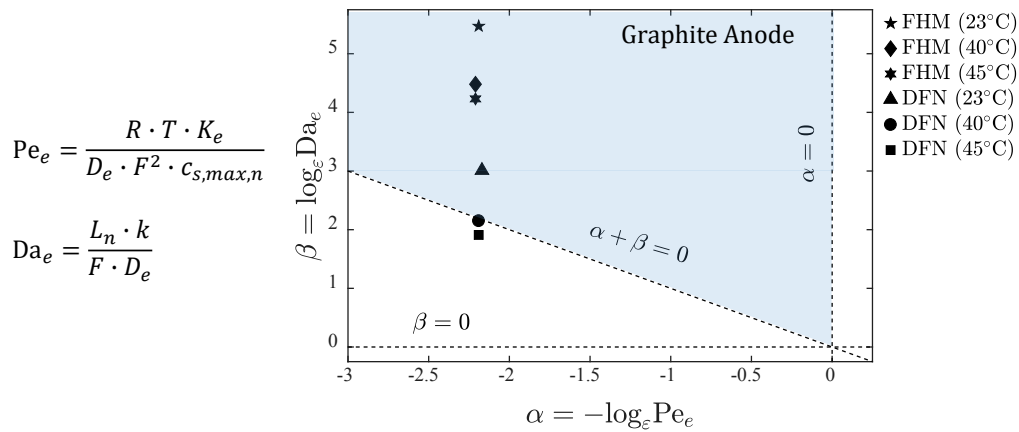


Fig. 3: Electrolyte phase diagram for the graphite anode. The data points represent  $(\alpha, \beta)$  values calculated for the DFN and FHM models. At temperatures higher than 40°C, the DFN model data points move outside the applicability regime.

higher temperatures of battery operation, there is a loss of accuracy in the DFN model towards the end of discharge. On the other hand, the FHM model predicts cell dynamics accurately until the end of the discharge curve.

An electrolyte phase diagram analysis was conducted to assess the validity of the applicability constraints of macroscale models in predicting cell behavior. The phase diagram approach was initially proposed by Battiato *et. al.* [25] to identify the conditions under which effective advection-dispersion-reaction equations provide an accurate description of the micro-scale transport processes. Introduced for the first time for lithium-ion batteries in [18], it is a powerful tool with the ability to indicate battery operating conditions under which the error in macroscale model predictiveness is bounded with respect to its pore-scale counterpart. The phase diagram implementation for different electrodes in a certain range of battery operating temperatures is detailed in [26], and an assessment of the veracity of macroscale models for batteries subject to capacity fading using the phase diagram is elaborated in [27].

Electrolyte diffusion and conductivity values were ob-

tained as a function of temperature from [19]. They were evaluated at the initial electrolyte lithium concentration of 1200 [mol/m<sup>3</sup>] for both models. The dimensionless Péclet and Damköhler numbers,  $Pe_e$  and  $Da_e$ , are computed for the graphite anode. The values of the phase diagram parameters  $(\alpha, \beta)$  for the DFN and FHM models are plotted for three cell temperatures: 23°C, 40°C, and 45°C, as shown in Fig. 3.

It can be observed from the phase diagram that the points  $(\alpha, \beta)$  of the DFN model violate the applicability constraint  $(\alpha + \beta \geq 0)$  at temperatures of 40°C and beyond. Under the same conditions, the points  $(\alpha, \beta)$  of the FHM model stay within the blue shaded region since they satisfy all the applicability constraints. When data points  $(\alpha, \beta)$  fall out of the applicability regime (defined by the blue shaded region), macroscale modeling electrolyte equation error is no longer bounded.

The loss in the predictability of the DFN model at 40°C and 45°C, as observed from Fig. 2, can be attributed to a violation of the constraints that enable successful upscaling of the macroscale transport equations. At higher operating temperatures, the dominance of reaction transport leads to the

formation of diffusion-limited regimes. Under these circumstances, the system is no longer well-mixed, and macroscopic transport models can become invalidated and incapable of capturing pore-scale dynamics.

## V. CONCLUSION

Accurate prediction of battery behavior across a wide range of operating temperatures and current rates of charge or discharge is dependent on a reliable description of battery internal transport processes. One of the major contributions of this paper is the identification of operating conditions under which the assumptions and approximations that facilitate the use of the DFN macroscale model are violated, leading to a loss of model predictability.

The results from the finite element implementation of the DFN model and the FHM model developed in [18] is presented in this paper. The performance of both the models were assessed using data from experimental measurements on 18650 cylindrical lithium-ion cells composed of NMC cathode and graphite anode. A cost function was designed to minimize the error between experimentally measured and model-predicted voltage response of the cell. The same geometric and stoichiometric parameters were used in both the models, and 5 temperature-dependent parameters were individually identified for both the models using constant current discharge experimental data sets.

The results of the identification studies and the phase diagram analysis indicate that the DFN model, which predicts battery dynamics well at 23°C, fails to replicate the same at temperatures greater than 40°C. This implies that significant caution must be exercised while implementing the DFN and its reduced-order formulations for applications where the battery operates over a wide range of SoC. A major contribution of this paper is the development and validation of the enhanced predictability of the FHM model, which can be used to develop advanced physics-based control strategies for BMS applications.

## VI. ACKNOWLEDGEMENT

The authors acknowledge the partial support of the National Science Foundation through the grant CAREER #1839050.

## REFERENCES

- [1] T. V. Johnson and A. Joshi, "Directions in vehicle efficiency and emissions," *Combustion Engines*, vol. 55, 2016.
- [2] B. Nykvist and M. Nilsson, "Rapidly falling costs of battery packs for electric vehicles," *Nature Climate Change*, vol. 5, no. 4, p. 329, 2015.
- [3] J. W. Choi and D. Aurbach, "Promise and reality of post-lithium-ion batteries with high energy densities," *Nature Reviews Materials*, vol. 1, p. 16013, 2016.
- [4] S. Al Hallaj, H. Maleki, J.-S. Hong, and J. R. Selman, "Thermal modeling and design considerations of lithium-ion batteries," *J. Power Sources*, vol. 83, no. 1, pp. 1–8, 1999.
- [5] K. A. Smith, "Electrochemical control of lithium-ion batteries," *IEEE Control Systems Magazine*, vol. 30, no. 2, pp. 18–25, 2010.
- [6] S. Malifarge, B. Delobel, and C. Delacourt, "Determination of Tortuosity Using Impedance Spectra Analysis of Symmetric Cell," *J. Electrochem. Soc.*, vol. 164, no. 11, pp. E3329–E3334, 2017.
- [7] L. Zheng, L. Zhang, J. Zhu, G. Wang, and J. Jiang, "Co-estimation of state-of-charge, capacity and resistance for lithium-ion batteries based on a high-fidelity electrochemical model," *Applied Energy*, vol. 180, pp. 424–434, 2016.
- [8] K.-J. Lee, K. Smith, and G.-H. Kim, "Three-Dimensional Thermal-Electrochemical Coupled Model for Spirally Wound Large-Format Lithium-Ion Batteries (Presentation)," tech. rep., National Renewable Energy Laboratory (NREL), Golden, CO., 2011.
- [9] M. Doyle, T. F. Fuller, and J. Newman, "Modeling of Galvanostatic Charge and Discharge of the Lithium/Polymer/Insertion Cell," *J. Electrochem. Soc.*, vol. 140, no. 6, pp. 1526–1533, 1993.
- [10] G. M. Goldin, A. M. Colclasure, A. H. Wiedemann, and R. J. Kee, "Three-dimensional particle-resolved models of li-ion batteries to assist the evaluation of empirical parameters in one-dimensional models," *Electrochim. Acta*, vol. 64, pp. 118–129, 2012.
- [11] J. Smekens, J. Paulsen, W. Yang, N. Omar, J. Deconinck, A. Hubin, and J. V. Mierlo, "A Modified Multiphysics model for lithium-ion batteries with a  $\text{Li}_x\text{Ni}_{1/3}\text{Mn}_{1/3}\text{Co}_{1/3}\text{O}_2$  electrode," *Electrochimica Acta*, vol. 174, pp. 615–624, 2015.
- [12] P. R. Shearing, L. E. Howard, P. S. Jørgensen, N. P. Brandon, and S. J. Harris, "Characterization of the 3-dimensional microstructure of a graphite negative electrode from a Li-ion battery," *Electrochemistry Communications*, vol. 12, no. 3, pp. 374–377, 2010.
- [13] A. Vadakkepat, B. Trembacki, S. R. Mathur, and Y. J. Murthy, "Bruggeman's exponents for effective thermal conductivity of lithium-ion battery electrodes," *J. Electrochem. Soc.*, vol. 163, no. 2, pp. A119–A130, 2016.
- [14] S. Santhanagopalan and R. E. White, "Online estimation of the state of charge of a lithium ion cell," *J. Power Sources*, vol. 161, no. 2, pp. 1346–1355, 2006.
- [15] T. R. Tanim, C. D. Rahn, and C. Y. Wang, "State of charge estimation of a lithium ion cell based on a temperature dependent and electrolyte enhanced single particle model," *Energy*, vol. 80, pp. 731–739, 2015.
- [16] H. Arunachalam, S. Korneev, I. Battiato, and S. Onori, "Multiscale modeling approach to determine effective lithium-ion transport properties," in *Proceedings of the 2017 American Control Conference*, pp. 92–97, IEEE, 2017.
- [17] G. L. Plett, *Battery Management Systems, Volume I: Battery Modeling*. Artech House, 2015.
- [18] H. Arunachalam, S. Onori, and I. Battiato, "On Veracity of Macroscopic Lithium-Ion Battery Models," *J. Electrochem. Soc.*, vol. 162, no. 10, pp. A1940–A1951, 2015.
- [19] L. O. Valoen and J. N. Reimers, "Transport Properties of LiPF<sub>6</sub>-Based Li-Ion Battery Electrolytes," *J. Electrochem. Soc.*, vol. 152, no. 5, pp. A882–A891, 2005.
- [20] M. Ebner, D. W. Chung, R. E. Garcia, and V. Wood, "Tortuosity Anisotropy in Lithium-Ion Battery Electrodes," *Advanced Energy Materials*, vol. 4, no. 5, 2014.
- [21] H. Arunachalam, "A New Multiscale Modeling Framework for Lithium-Ion Battery Dynamics: Theory, Experiments, and Comparative Study with the Doyle-Fuller-Newman Model," 2017.
- [22] S. Ebbesen, P. Kiwiz, and L. Guzzella, "A generic particle swarm optimization matlab function," in *Proceedings of the 2012 American Control Conference*, pp. 1519–1524, IEEE, 2012.
- [23] J. Li, L. Zou, F. Tian, X. Dong, Z. Zou, and H. Yang, "Parameter Identification of Lithium-Ion Batteries Model to Predict Discharge Behaviors Using Heuristic Algorithm," *J. Electrochem. Soc.*, vol. 163, no. 8, pp. A1646–A1652, 2016.
- [24] J. C. Forman, S. J. Moura, J. L. Stein, and H. K. Fathy, "Genetic identification and fisher identifiability analysis of the Doyle-Fuller-Newman model from experimental cycling of a LiFePO<sub>4</sub> cell," *J. Power Sources*, vol. 210, pp. 263–275, 2012.
- [25] I. Battiato and D. M. Tartakovsky, "Applicability regimes for macroscopic models of reactive transport in porous media," *J. Contam. Hydrol.*, vol. 120-121, pp. 18–26, 2011.
- [26] H. Arunachalam, S. Onori, and I. Battiato, "Temperature-dependent multiscale-dynamics in Lithium-ion battery electrochemical models," in *Proceedings of the 2015 American Control Conference*, pp. 305–310, IEEE, 2015.
- [27] H. Arunachalam, I. Battiato, and S. Onori, "Preliminary investigation of provability of li-ion macroscale models subject to capacity fade," in *Proceedings of the 2016 Dynamic Systems and Control Conference*, ASME, 2016.